AIP | Review of Scientific Instruments

A Mo-anode-based in-house source for small-angle X-ray scattering measurements of biological macromolecules

Linda K. Bruetzel, Stefan Fischer, Annalena Salditt, Steffen M. Sedlak, Bert Nickel, and Jan Lipfert

Citation: Review of Scientific Instruments **87**, 025103 (2016); doi: 10.1063/1.4940936
View online: http://dx.doi.org/10.1063/1.4940936
View Table of Contents: http://scitation.aip.org/content/aip/journal/rsi/87/2?ver=pdfcov
Published by the AIP Publishing

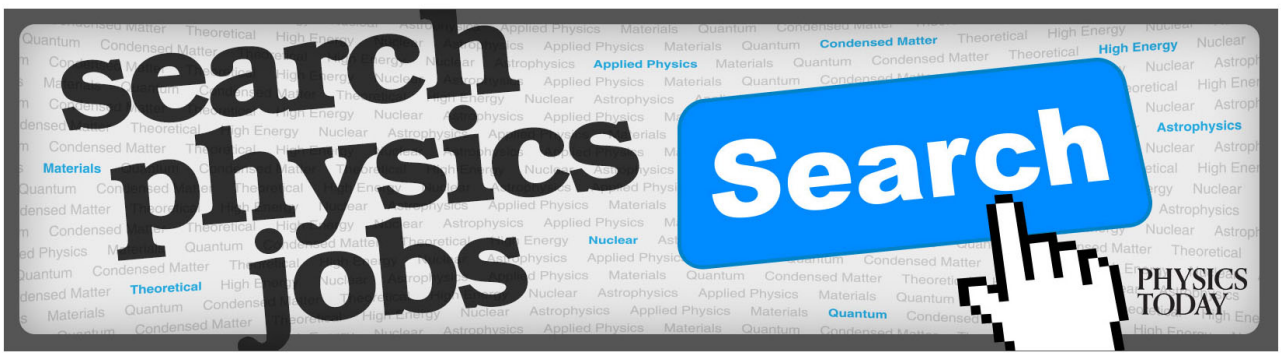

A Mo-anode-based in-house source for small-angle X-ray scattering measurements of biological macromolecules

Linda K. Bruetzel, Stefan Fischer, Annalena Salditt, Steffen M. Sedlak, Bert Nickel, and Jan Lipfert[a)]

Department of Physics, Nanosystems Initiative Munich, and Center for Nanoscience, Ludwig-Maximilians-University Munich, Amalienstr. 54, 80799 Munich, Germany and Geschwister-Scholl Platz 1, 80539 Munich, Germany

(Received 17 November 2015; accepted 15 January 2016; published online 8 February 2016)

We demonstrate the use of a molybdenum-anode-based in-house small-angle X-ray scattering (SAXS) setup to study biological macromolecules in solution. Our system consists of a micro-focus X-ray tube delivering a highly collimated flux of 2.5×10^6 photons/s at a beam size of 1.2×1.2 mm^2 at the collimation path exit and a maximum beam divergence of 0.16 mrad. The resulting observable scattering vectors q are in the range of 0.38 Å^{-1} down to 0.009 Å^{-1} in SAXS configuration and of 0.26 Å^{-1} up to 5.7 Å^{-1} in wide-angle X-ray scattering (WAXS) mode. To determine the capabilities of the instrument, we collected SAXS data on weakly scattering biological macromolecules including proteins and a nucleic acid sample with molecular weights varying from ~12 to 69 kDa and concentrations of 1.5–24 mg/ml. The measured scattering data display a high signal-to-noise ratio up to q-values of ~0.2 Å^{-1} allowing for an accurate structural characterization of the samples. Moreover, the in-house source data are of sufficient quality to perform *ab initio* 3D structure reconstructions that are in excellent agreement with the available crystallographic structures. In addition, measurements for the detergent decyl-maltoside show that the setup can be used to determine the size, shape, and interactions (as characterized by the second virial coefficient) of detergent micelles. This demonstrates that the use of a Mo-anode based in-house source is sufficient to determine basic geometric parameters and 3D shapes of biomolecules and presents a viable alternative to valuable beam time at third generation synchrotron sources. © *2016 AIP Publishing LLC.* [http://dx.doi.org/10.1063/1.4940936]

I. INTRODUCTION

Small-angle X-ray scattering (SAXS) is a powerful tool to investigate the structure and interactions of biological macromolecules in solution.[1–3] SAXS has the important advantage of being a solution-based technique, thus obviating the need for sample crystallization and enabling studies of biological macromolecules in a range of solution conditions, from (near-) physiological to highly denaturing.[4] In the past, SAXS data have frequently been used to determine basic parameters of macromolecules in solution, such as the radius of gyration[5,6] (R_g) and the maximum intramolecular distance[7] (D_{max}). Determination of, e.g., R_g under varying solution conditions has provided important insights into protein[4] and RNA folding[8] and into the nature of the unfolded states.[9,10] Nonetheless, the utility of SAXS data has been tremendously enhanced in the last two decades through the increasing availability of algorithms to determine and to compare the (low resolution) 3D structures of macromolecules from 1D scattering profiles. In particular, a number of algorithms now make it possible to obtain low resolution 3D "bead" models from SAXS data for proteins[11–13] and for nucleic acids[14] without any other prior information about the sample. In addition, if SAXS data can be combined with prior information from, e.g., FRET,[15] NMR,[16] crosslinking, or known crystal structures[3,6] even more refined molecular models can be obtained.

Current SAXS measurements often rely on state-of-the-art synchrotron sources, in particular, due to their high photon flux and tunability. Nonetheless, in-house anode-based sources remain an important and attractive alternative,[17] in particular, given the limited availability of measurement time at synchrotron user facilities and the considerable logistic challenges to carry out measurements at an-often far away-off-site location. In principle, it is possible to compensate the reduced flux at lab-sources at least partially by extended counting times, e.g., by increasing exposure times from ~1 s typical for biological samples at high-flux synchrotrons to 10^3–10^4 s. However, this approach only works if the signal-to-noise ratio is high, i.e., if the background noise does not increase too much for long integration times. Therefore, the question which energy range is best suited for SAXS measurements of macromolecules in solution is tightly connected to the question which energy range provides the best signal-to-noise ratio for these conditions.

Currently, most in-house based sources employ copper (Cu) anodes with K_α radiation at 8.0 keV, corresponding to a wavelength of 1.54 Å. Their application for solution SAXS measurements on weakly scattering biological samples has been already proven[17] and also *ab initio* reconstructions with

a)Author to whom correspondence should be addressed. Electronic mail: Jan.Lipfert@lmu.de

the programs DAMMIF[18] and GASBOR[12] could be performed successfully.[19,20] An alternative to Cu anodes are molybdenum (Mo; K_α = 17.4 keV) anode sources, which provide shorter wavelength X-rays compared to Cu, with a characteristic wavelength of 0.71 Å. Mo-anode sources have been employed to investigate macromolecules, powders or thin film alloys by SAXS,[21] wide-angle X-ray scattering (WAXS),[21–23] grazing-incidence X-ray scattering (GISAXS),[24] crystallography,[25] and diffractometry.[26,27] However, a detailed description and analysis of a Mo-anode-based in-house setup for SAXS measurements on biological macromolecules in solution is still lacking. Here, we present a comprehensive specification and characterization of a Mo-anode in-house source for SAXS measurements on proteins, nucleic acids, and detergent micelles. The shorter wavelength of Mo has a number of potential advantages: First, since the absorption coefficient for X-rays decreases sharply with increasing energy, higher energies cause less radiation damage in the sample.[28] Second, scattering from air and window materials in the beam path is also reduced at higher X-ray energies. Third, the reduced absorption coefficient means that the optimal beam path (μ^{-1}) in the sample is longer for higher X-ray energies, e.g., for water μ^{-1}~10 mm for Mo and μ^{-1}~1 mm for Cu radiation, which can be advantageous for samples handling, i.e., for sample environments that benefit from larger sample dimensions. Fourth, since the magnitude of the scattering vector q is inversely proportional to the X-ray wavelength λ, a shorter wavelength is highly beneficial to perform WAXS measurements, where high q values are desired. Thus, a shorter wavelength as given by Mo anodes, facilitates the combination of SAXS and WAXS measurements within a single setup, which can be advantageous for structural studies on biological samples such as proteins or peptides.[29,30]

We test our Mo-anode setup on a panel of typical, weakly scattering biological samples, including several proteins (bovine serum albumin, horse heart cytochrome *c*, and chicken egg white lysozyme), a nucleic acid sample (24 bp DNA duplex), and a micelle forming detergent (decyl-maltoside; DM). These samples have been investigated previously at third generation synchrotron sources and (except for the micelle sample) have known crystallographic structures, enabling a critical comparison and evaluation of our in-house data. The results suggest that our Mo-anode-based source achieves good signal-to-noise even on weakly scattering samples; the data are of sufficient quality to carry out standard SAXS analyses, such as Guinier fitting of the R_g, and to obtain *ab initio* 3D shape reconstructions for the protein and nucleic acid samples that exhibit good agreement with the known crystallographic structures. In addition, the data permit to fit a two-component ellipsoid model to the DM micelle data and to determine the size, shape, and interactions of the detergent micelles in solution.

II. THE X-RAY SETUP

In brief, the in-house setup consists of a microfocus X-ray source with multilayer optics corresponding to the K_α line of the target, a collimation path with two scatterless slits, a motorized sample stage, two exchangeable vacuum tubes, and a hybrid pixel detector (Fig. 1). The individual components are described in detail in Secs. II A–II E. The setup is optimized for SAXS measurements but can also be used for WAXS and diffraction measurements, as shown previously[31] and discussed only briefly here.

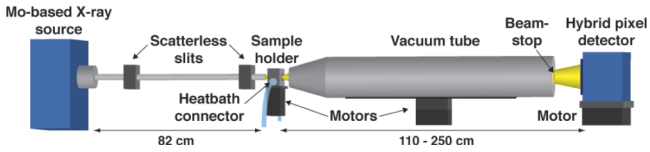

FIG. 1. Schematic layout of the in-house setup for SAXS measurements. For further details see Section II in the text.

A. X-ray source and collimation path

Our system consists of a Mo GeniX^{3D} microfocus X-ray tube (Xenocs SA, Sassenage, France) combined with FOX2D single reflection optics delivering a monochromatic and highly stable beam with an X-ray energy of 17.4 keV. The flux is typically around 2.5×10^6 photons/s at the sample stage. For collimation the beam enters an 82 cm long, fully evacuated collimation path closed by a 25 μm thick Kapton foil at the end. Collimation is achieved by integrating two partially motorized scatterless aperture slits (Xenocs SA, Sassenage, France),[32] one upstream right at the mirror and the second at the tube exit. The scatterless slits consist of a rectangular single Ge-crystal substrate bonded to a metal base with a large tapering angle away from the beam, which significantly reduces parasitic scattering and enhances resolution compared to conventional X-ray apertures.[32] Moreover, their insertion leads to a simplified optical design in comparison to previous implementations, which required three apertures.[33] With this optical configuration, we achieve a highly collimated (horizontal divergence: 0.12 mrad, vertical divergence: 0.16 mrad FW20%M) beam with a size of approximately 1.2×1.2 mm^2 at the collimation path exit.

B. Sample cell and sample stage

The sample stage is positioned 5 cm in front of the collimation path exit. It consists of a fully motorized platform where six stepper motors allow moving the stage in horizontal and vertical directions with 5 μm and 0.1 μm precision, respectively, and enable rotation of the stage about all three axes with 0.005° precision. A rectangular aluminum sample holder with two slots for sample chambers (adapted from Ref. 34) is connected to the platform for successive automated measurements of sample and buffer solution (Fig. S1 of the supplementary material).[35] The bottom part of the sample holder is connected to a circulating water bath (F12-MA, Julabo, Germany) via rubber tubes enabling temperature control of the sample cells in the range of 4–70 °C (±0.8 °C). For SAXS measurements conducted at room temperature, we used polyvinyl chloride (PVC) based sample chambers. The cylindrical observation volume of the chambers is filled with sample solution via two small inlets with a diameter of 0.6 mm from the top. This design prevents the formation of air bubbles and minimizes evaporation during measurements. In

order to achieve the optimum scattering signal, the chamber length corresponds to the absorption length of Mo in water, equal to the absorption coefficient, which is approximately 10 mm[36] The diameter of the cylindrical observation volume is 3 mm so that parasitic scattering due to interactions of the incoming beam with the PVC is avoided and the opening angle is large enough so that scattering events happening at the beginning of the chamber can still be detected. The overall sample volume is roughly 80 μl. The windows of the sample chamber are made of 25 μm thick potassium aluminosilicate (muscovite mica) sheets (Goodfellows Cambridge Ltd., UK) that are glued on both openings of the cell with two-component epoxy (UHU Ltd., Germany). The use of mica as window material only introduces ~6% attenuation (assuming an attenuation length of 800 μm for mica[36]) and it suppresses evaporation of sample solution during measurements. Furthermore, the windows do not cause a detectable background signal (see the text and Fig. S2 of the supplementary material).[35] For temperature-controlled experiments, we used sample chambers made from aluminum for improved thermal coupling. The sample holder can be removed to perform calibration measurements with glassy carbon, silver behenate (AgBe), and lanthanum hexaboride (LaB_6). AgBe and LaB_6 are stored in aluminum chambers closed by 25 μm thick Kapton foils. The glassy carbon sample is fixed in an aluminum holder and mounted directly below the AgBe chamber. The calibration materials can be placed into the beam by a motor.

C. Evacuated flight path and beamstop

Our setup for SAXS measurements can be switched between two sample-detector distances of 110 cm and 250 cm, corresponding to q-ranges of 0.014–0.38 Å^{-1} and 0.009–0.15 Å^{-1}, respectively. A distance of 250 cm corresponds to more pixels covering the low q-range. For the two measurement modes, vacuum tubes with lengths of 95 cm and 180 cm, respectively, are placed between the sample stage and the detector in order to reduce air scattering (Fig. 1). A detailed analysis of various sources of background signals and, in particular, of the influence of air scattering on the SAXS data is given in the text and Fig. S2 of the supplementary material.[35] Kapton foils with a thickness of 25 μm at the front and 50 μm at the end seal the ends of each vacuum tube. The vacuum tube has a diameter of 3 cm at the front and 10 cm at the back. We integrate beamstops at the end of the vacuum tubes by gluing circular lead tapes with diameter of 3 mm (for the 95 cm vacuum tube) and 4 mm (for the 180 cm vacuum tube) at the center of the Kapton foil inside the vacuum tube. The entire vacuum tube can be moved by two stepper motors in vertical and horizontal directions allowing for accurate alignment of the beamstop. This configuration is advantageous, as it does not introduce any additional shadow effects from a beamstop holder, and as it avoids air scattering compared to a beamstop positioned outside of the vacuum. Moreover, the lead tape is slightly transparent to the beam so that fluctuations in the beam position can be detected. In the WAXS geometry, the sample-to-detector distance is set to 32 cm resulting in a q-range of 0.26–5.7 Å^{-1}. Due to the relatively short sample-to-detector distance, we do not employ an evacuated flight path.

D. Detector

For X-ray detection, we use a CMOS hybrid pixel detector (Pilatus 100K, Dectris Ltd, Switzerland) with a sensor thickness of 1000 μm yielding a quantum efficiency at molybdenum K_α-energy of 76%, which is limited by the absorption of silicon (μ^{-1} (Mo) ~700 μm for silicon). The detector area consists of 487×195 pixels with a pixel size of 172 μm in both directions, which leads to a total size of 83.8×33.5 mm^2 (width $\times$ height). The dynamic range is 20 bits, corresponding to 1 048 576 photons. Hybrid pixel detectors are single photon counters with the advantage of low background and the absence of dark noise.[37] For the SAXS configuration with the short vacuum tube, the detector is attached to a stepper motor that moves the detector in vertical direction. This stepper motor is fixed to a custom-made focusing rail, which can be moved manually in order to align the detector in the horizontal direction. For the configuration with the long sample-detector distance, the detector is fixed in vertical position such that the beam is centered and can be adjusted manually in the horizontal dimension. For WAXS measurements, the detector is placed on a motorized stage (BiSlide, Velmex, Inc.). The motorized stage can be moved in horizontal and vertical direction with a travel range of 25.4 cm for automated scanning and stitching of the detector images.

E. Software

We control the instrument components and perform data acquisition using the UNIX-based software package "spec" (Certified Scientific Software, Cambridge, USA) which is widely used for X-ray scattering and diffraction experiments at synchrotrons and laboratory systems. The "spec" can directly communicate with the Pilatus detector via macros (downloaded from the Dectris website: www.dectris.com). Furthermore, a custom-written Matlab routine displays the live image of the detector for fast and easy adjustment.

III. MATERIALS AND METHODS

A. Calibration standards

We utilize silver behenate (AgBe; VWR International, Germany) to calibrate the beam center position and sample-to-detector distance for all small-angle measurements (Fig. S3 of the supplementary material).[35,38] In addition, we use a pre-calibrated 1 mm thick glassy carbon sample (kindly provided by Dr. Jan Ilavsky, APS, Argonne National Laboratory, USA) for the calibration of the recorded intensity to absolute scattering cross section units[39] of cm^{-1} and sr^{-1}, which enables the comparison of scattering data from different instruments. For the calibration of the wide-angle configuration, we use lanthanum hexaboride (LaB_6; SRM 660c, NIST) (Fig. S3 of the supplementary material).[35]

TABLE I. Overview of samples with corresponding concentrations and buffers used for SAXS measurements.

Sample	Number of residues/nucleotides	Molecular weight (kDa)	Concentrations (mg/ml)	Buffer
BSA	583	69.0	5	50 mM HEPES, pH = 7.5, 50 mM KCl
Cytochrome *c*	104	12.4	2, 8, 24	100 mM acetate buffer, pH = 4.6, 0.5M guanidinium hydrochloride
Lysozyme	129	14.3	5, 10, 20	40 mM acetate buffer, pH = 4.5, 150 mM NaCl
24 bp DNA duplex	48	~14.6	1.5, 4.4	50 mM sodium 3-(*N*-morpholino) propanesulfonic acid, pH = 7.0, 150 mM NaCl

B. Sample preparation

A 24 bp DNA duplex sample was assembled from chemically synthesized oligonucleotides (Metabion, Germany) and prepared as described previously.[40] Bovine serum albuminum (BSA), cytochrome *c*, and lysozyme were purchased from Sigma-Aldrich and used without further purification. Detailed information about the employed buffers and sample concentrations is listed in Table I. For concentration series, a stock solution of the highest concentration was prepared by weighing out the lyophilized protein powder and diluted to the required concentrations. Both buffer and sample solutions were filtered through 0.22 μm syringe filters (Thermo scientific, USA). Prior to the measurements, sample solutions were centrifuged at 13 500 rpm for 10 min in a tabletop centrifuge (Eppendorf, Germany). Sample and buffer solutions were degassed in a desiccator at a pressure level of 30 mbar for 20 min to avoid the formation of air bubbles in the sample chamber during measurements. For each measurement, 80 μl of sample or buffer solution was loaded into the sample chambers.

C. Measurement procedures

Prior to each experimental run, scattering curves of AgBe and glassy carbon were measured to determine the sample-detector distance with mm-accuracy and to calibrate the scattering curves on an absolute scattering scale. Sample chambers were placed in the sample holder and aligned such that the incoming X-ray beam penetrates the chamber at its center as follows: The sample stage is scanned vertically and horizontally in a range of 5 mm. At each position, a 1 s exposure is recorded with the beamstop removed and the intensity is integrated. The intensity stays approximately constant when the X-ray beam penetrates the observation volume and drops off rapidly when the beam is clipped by the sides of the sample chamber, allowing for an accurate determination of the center position.

Biological SAXS measurements were performed at room temperature and exposure times were set to 1–3 h with 3–6 repeats each, resulting in a total exposure time of up to 24 h for each measurement. Matching SAXS profiles of each repeat were used for data averaging as described in Sec. III D. For concentration series, we used the same chamber, which was rinsed with deionized water and buffer solution before filling it with fresh sample solution. Matching buffer profiles were collected using identical settings and procedures. For selected SAXS experiments, dynamic light scattering measurements on a NANO-flex® 180° instrument (Particle Metrics GmbH, Germany) were performed to test for possible aggregation. No aggregation was observed for any of the tested samples.

D. Data processing and evaluation

The two-dimensional detector images were processed with a macro including the command "remove outliers" of the software ImageJ (National Institutes of Health, USA) in order to remove artefacts, which appear as small bright spots of only a few pixels in the detector image, due to background radiation as, for instance, cosmic rays. The "remove outliers" algorithm replaces a pixel value by the median of adjacent pixel values if it deviates from the median by more than the threshold value. We used a radius of 7 for the pixel area to calculate the median and a threshold value of 50. By setting "which outlier" to "bright" only pixels that are brighter than the median of the surrounding are replaced. Next, we used the Igor Pro plugin NIKA[41] to reduce the 2D detector data into a one-dimensional scattering intensity. First, the sample-to-detector distance and the beam center were refined based on the AgBe scattering data. Then, circular averaging of both sample and buffer images was performed without any additional corrections. We further used custom-written MATLAB scripts to inspect the scattering data for aggregation or radiation damage, to perform data averaging, buffer subtraction, to define the usable q-range and for calibration of the data to exposure time, concentration, and absolute intensity. In addition, the MATLAB scripts performed a Guinier analysis to determine the radius of gyration (R_g) by iterative linear regression within the q-range of the data limited by $q \cdot R_g < 1.3$. Unless otherwise noted, the profiles shown represent averaged scattering data resulting from 3 repeats of 2 h exposures.

E. Theoretical scattering curves and *ab initio* low resolution reconstructions

For comparison of the experimental SAXS data, we calculated theoretical scattering profiles for our panel of scattering standards based on their atomic coordinates using the program *CRYSOL*[42] in default mode. The crystallographic structures of the protein samples were obtained from the protein data bank,[43] with PDB accession codes 4F5S for BSA, 1HRC for cytochrome *c* and 6LYZ for lysozyme. For the 24 bp DNA, a PDB file with the atomic coordinates was generated using the 3DNA package.[44]

We used the program DAMMIF[18] to generate *ab initio* three-dimensional models from the scattering data. DAMMIF represents the particle as an assembly of identical beads

inside a search volume. It employs a simulated annealing protocol to determine a compact interconnected model whose scattering pattern fits the experimental data. The particle distance distribution function $P(r)$ generated from the ATSAS software[45] was used as input file. For each tested molecule, 20 independent runs in the "slow" mode were performed using default parameters and assuming no symmetry. Next, we averaged the 20 models for each molecule using DAMAVER[46] comprising a sequence of programs: first, the low resolution models from DAMMIF were aligned based on their axes of inertia using a normalized spatial discrepancy (NSD) criterion.[47] The NSD value provides a quantitative measure of similarity between different models. A NSD value of zero corresponds to identical objects and values exceeding 1 refer to objects that systematically differ from one another. If pairwise NSD values are in the range between zero and one then the models are classified as structurally similar. The aligned bead models were averaged and filtered by removing loosely connected beads. For the next steps, the reconstructed file with the lowest NSD value was chosen. We used the pdb2vol program from the SITUS[48] package (version 2.7.2) to convert aligned bead models to electron density maps. Finally, we aligned the models to the corresponding crystal structures,[43] again by minimizing the NSD value between both structures. Molecular graphics were prepared using visual molecular dynamics.[49]

IV. RESULTS AND DISCUSSION

To explore the capabilities of our setup, we conducted a number of test measurements using a panel of biological macromolecules as measurement standards that comprise horse heart cytochrome *c*, chicken egg white lysozyme, BSA, and a 24 bp DNA construct (Table I). All selected macromolecules have known high-resolution structures and have been used as scattering standards previously.[14,50–52] They span a range of molecular weights but, in general, have relatively small sizes and, consequently, scatter weakly. Therefore, they are ideally suited to characterize our setup within the described q-range and constitute rigorous test cases for typical biological samples for SAXS measurement.

A. Exposure time and concentration analysis

We initially carried out a set of test measurements to determine concentration requirements, optimal exposure times, and possible radiation damage effects. We performed concentration- and exposure time series on the scattering standard samples listed in Table I (except for BSA). Fig. 2(a) shows SAXS profiles for three different concentrations (5 mg/ml, 10 mg/ml, and 20 mg/ml) of lysozyme, which has been previously characterized in synchrotron based SAXS experiments.[10,52] The concentration scaled data are superimposable and exhibit no evidence of radiation damage or interparticle effects such as aggregation or interparticle interference. Kratky plots, where the scattering intensity weighted by q^2 is plotted against q, are shown for all concentrations (Fig. 2(b)). The Kratky representation is frequently used to represent scattering data of macromolecular ensembles,[4] where a well-folded homogeneous particle will exhibit a parabolic curve and an unfolded particle will give rise to a hyperbolic curve. For all three concentrations of lysozyme, the scattering profiles display a pronounced peak indicating that the protein is well-

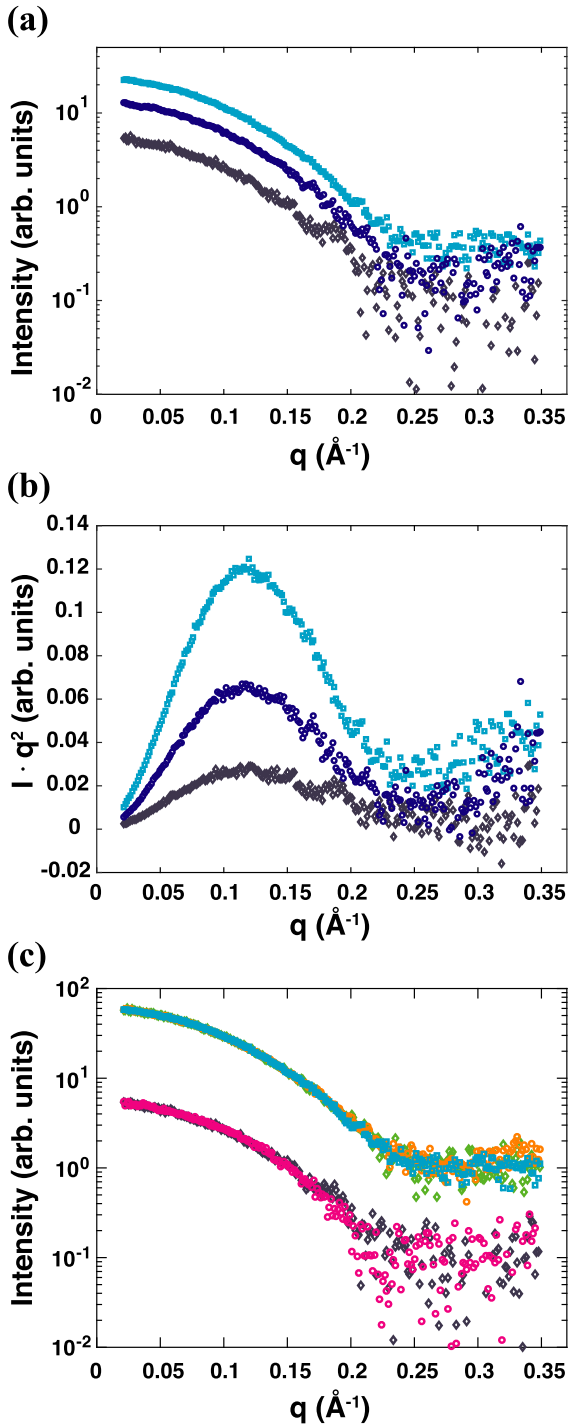

FIG. 2. Effects of protein concentration and exposure time on scattering profiles. Scattering profiles shown are for lysozyme (see Table I for details). (a) Averaged scattering data at concentrations of 20 mg/ml (cyan, squares), 10 mg/ml (blue, circles), and 5 mg/ml (grey, diamonds) for three repeats of 2 h. (b) Kratky plots ($q^2 \cdot I$ vs. q) for the data from panel (a). (c) Averaged scattering data of lysozyme at a concentration of 20 mg/ml for six repeats of 0.5 h (green, diamonds), three repeats of 1 h (orange, circles) and two repeats of 2 h (cyan, squares) and a concentration of 5 mg/ml with exposure times of 2 h for three repeats (grey, diamonds) and 3 h for two repeats (magenta, circles). Data are scaled by exposure time.

behaved in its folded state. Although the signal-to-noise ratio decreases for lower concentrations, we still obtain reasonable quality data at the lowest concentration of 5 mg/ml. In addition, we examined different exposure times and number of repeats for the highest and lowest concentrations used for our test molecules (Fig. 2(c)). We found that for lysozyme (c = 20 mg/ml) six exposures of 30 min each lead already to decent signal for q-values below 0.2 Å^{-1}. However, we observed an improvement in data quality when using three repeats of 2 h, resulting in a signal-to-noise ratio suitable for structural analysis as described in Section IV C. Even longer exposure times were tested for the lowest concentration but did not increase the data quality. This is probably due to a higher level of background noise attributed to background radiation, which is also integrated over time. Similar results were obtained for cytochrome c measured at concentrations of 2, 8, and 24 mg/ml (Fig. S4 of the supplementary material).[35]

B. Comparison of in-house data and synchrotron data

We compared the data obtained at our in-house source with data collected at the beamline BM29 at the ESRF in Grenoble (for proteins) and at the beamline 12-ID-B of the Advanced Photon Source (APS), Argonne, Illinois (for the 24 bp DNA), both third generation synchrotron light sources with instruments designed for biological SAXS measurements in solution (Fig. 3). ESRF data were collected in the "flow" mode at room temperature with an exposure time of 1 s. APS data were collected in a static sample cell at room temperature with an exposure time of 1 s. Matching data from ten runs were averaged. For q values <0.2 Å^{-1}, the synchrotron scattering profiles are closely approximated by those acquired on the in-house setup. However, for larger q values, the signal-to-noise ratio decreases faster for the in-house data, as one would expect.

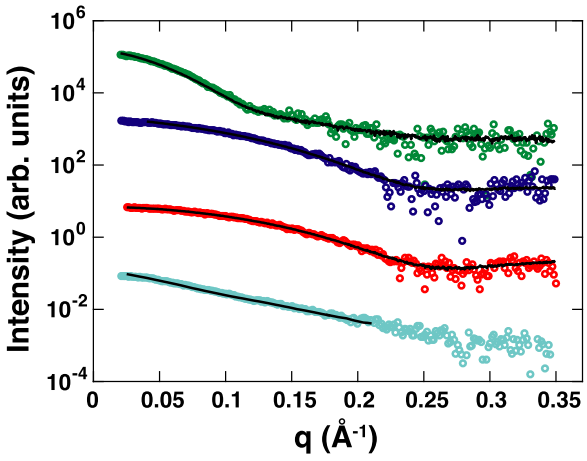

FIG. 3. Comparison of in-house source and synchrotron-based SAXS data. Scattering profiles acquired at our in-house source (shown in color) and measured at synchrotron sources (shown as black lines) for BSA (green, top), lysozyme (blue), cytochrome c (red), and 24 bp DNA (cyan, bottom) with concentrations from Table II. In-house data correspond to averaged data from three repeats with 2 h exposure time. Synchrotron data were averaged from 10 runs with 1 s exposure time. The synchrotron data for lysozyme had to be cut at a q-value of 0.04 Å^{-1} due to problems with the flow cell. DNA data were taken at another beamline with a maximum q-value of 0.21 Å^{-1}. Profiles are vertically offset for clarity.

C. Structural characterization and *ab initio* modeling of proteins and nucleic acids

The radius of gyration (R_g) and forward scattering intensity at zero angle ($I(0)$) are two parameters routinely extracted from SAXS data by Guinier analysis, where a straight line is fitted to the logarithm of the scattering intensity plotted as a function of q^2 for the lowest scattering angles. The R_g gives an overall measure for the size of the molecule; $I(0)$ is used to calculate the molecular weight (MW) and to evaluate sample monodispersity.[1,6] We performed Guinier analyses of the scattering profiles for every concentration and exposure time (see Fig. 4 for examples). For the molecular weight determination we employed BSA as reference sample. The Guinier plots for all of our test samples exhibit good linearity (Fig. 4) and the forward scattering intensities scale linearly with sample concentration, indicating the absence of interparticle interference effects or aggregation. We obtained radii of gyration from our experimental data that are consistent with literature values reported for the native state of each tested macromolecule (Table II). Molecular weight estimates from the forward scattering (Table II) are in good agreement (within experimental error) with the molecular weights expected from the primary structure of the monomeric samples. The error of the molecular weight determination in Table II is dominated by uncertainties in the macromolecular concentrations of approximately 10% relative error.

For further comparison, we calculated theoretical scattering profiles from the crystal structures (Figs. 5(a)-5(d)) for each tested molecule and determined the radius of gyration from the predicted scattering profiles based on the crystal structures (Table II). The experimental data are in excellent agreement with the theoretical scattering profiles and the overall scattering features of each molecule are observable. The resulting chi-squared values (χ^2), which characterize the "goodness-of-fit," are all around 0.1. Moreover, the

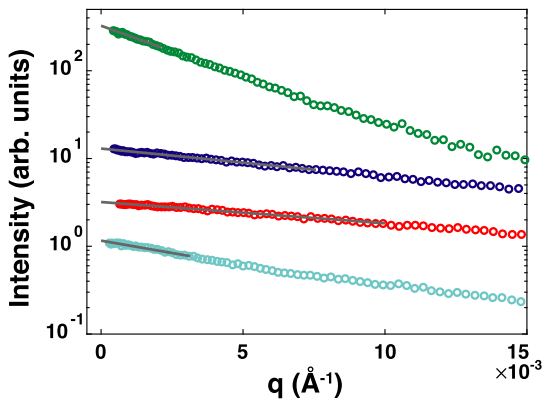

FIG. 4. Guinier analysis of biological samples. Guinier representation of the experimental scattering data for BSA (green, top), lysozyme (blue), cytochrome c (red) and 24 bp DNA (cyan, bottom). The Guinier fits are indicated by grey lines covering a q-range of $qR_g < 1.3$. Profiles are vertically offset for clarity.

TABLE II. Radii of gyration and molecular weights for protein and nucleic acid samples used in this study.

Sample	PDB used	Concentration (mg/ml)	R_g (Å)[a]	R_g (Å)[b]	R_g (Å)[c]	R_g (Å)[d]	MW[a] (kDa)	MW[b] (kDa)
BSA	4F5S	5	29.0 (±0.8)	29.9 (±0.8)[52]	27.3	28.1	...	69.0
Cytochrome *c*	1HRC	8	13.4 (±0.1)	13.8 (±0.3)[53]	12.6	13.2	11.5 (±1.1)	12.4
Lysozyme	6LYZ	10	14.6 (±0.4)	14.3 (±0.4)[52]	14.6	14.7	14.8 (±1.3)	14.3
24 bp DNA	...	1.5	23.3 (±2.7)	24.2 (±0.5)[14]	24.8	21.8	15.5 (±2.5)	14.6

[a]Values for radii of gyration and molecular weights determined in this study.
[b]Taken from experimental data reported in the literature.
[c]Calculated from the theoretical scattering profiles.
[d]From the reconstruction fit files.

theoretically predicted R_g values are in the range of the experimental and the literature values for all test samples.

Over the last two decades, the development of algorithms for *ab initio* reconstructions of low resolution three-dimensional electron density maps from one-dimensional scattering profiles has significantly enhanced the capabilities of SAXS measurements.[11–13,54] In addition, *ab initio* reconstructions can be combined with atomistic structures derived by NMR or X-ray crystallography or other sources of structural information to enhance or validate models for both proteins and nucleic acids.[14,55,56] To determine whether the data collected at our Mo-based in-house source are of sufficient quality to obtain 3D structure reconstructions of typical biological macromolecules, we performed *ab initio* modeling for all macromolecules of our test panel using the software DAMMIF (see Sec. III). The reconstructions converged to solutions that fit the experimental scattering profiles very well (Figs. 5(a)-5(d)). The scattering profiles from the models are in very good agreement with the experimental data over the whole q-range with χ^2 values below 0.1. However, they slightly deviate from the theoretical scattering profiles of the crystal structures for q-values above 0.25 Å^{-1}. For all reconstructions, the pairwise NSD values for independent reconstruction runs never exceeded 1, indicating that the reconstruction algorithm is stable and converges onto similar structures in each run. The final *ab initio* generated models were compared and aligned to corresponding crystal structures. Figs. 5(e)-5(h) show the bead models of each molecule rendered as smooth transparent surfaces and the superimposed crystal structures as black ribbons (proteins) and stick (24 bp DNA duplex) representations. The overall shapes and sizes of the proteins were reproduced well. For BSA (Fig. 5(e)), the reconstructed density fits nicely to the triangular-like shape of the protein. The surface of the density map is rough with several small indentations reproducing the high amount of alpha-helices present in native BSA. For lysozyme and cytochrome *c* (Figs. 5(f) and 5(g)), we obtained reconstructions representing their globular shape, which are in good agreement with the protein sizes. The reconstructed density of the 24 bp DNA duplex (Fig. 5(h)) corresponds reasonably to the overall cylindrical shape of a duplex. The length of the duplex gets reproduced well, whereas small deviations for the diameter of the reconstructions are observable. However, the periodicity of the major and minor grooves is visible in the reconstruction.

D. Determining the shape, size, and interactions of detergent micelles

Micelles are aggregates of amphiphilic molecules in aqueous solution where the hydrophilic head groups face

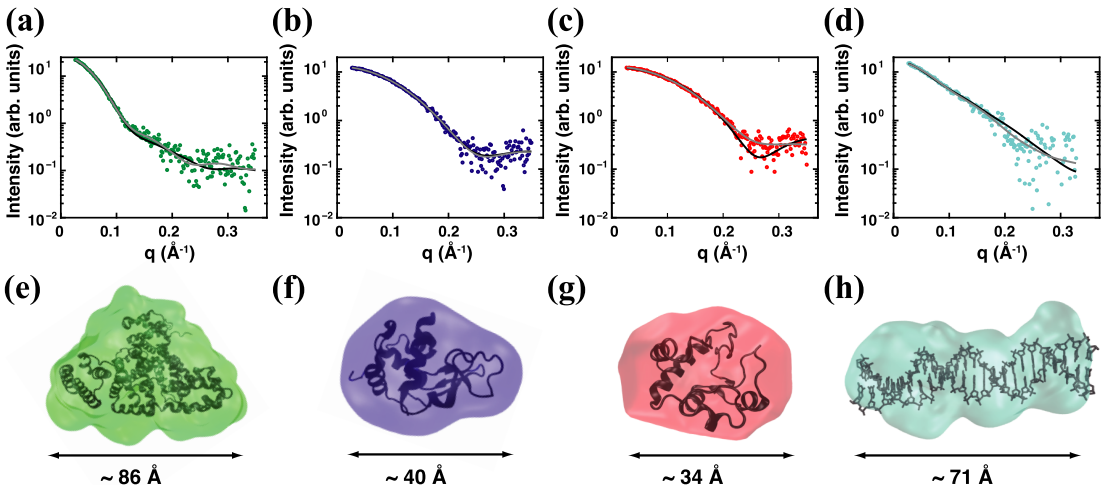

FIG. 5. Comparison of crystal structures and *ab initio* 3D shape reconstructions for protein and DNA samples. (a)-(d) Comparison of experimental (colors; same color code as in Figs. 3 and 4) and theoretical scattering profiles that were predicted from the crystal structures (black lines) and fitted scattering profiles from *ab initio* 3D reconstructions (grey lines). (e)-(h) Models obtained from *ab initio* 3D structure reconstructions for BSA (green), lysozyme (blue), cytochrome *c* (red), and 24 bp DNA (cyan). The maximum dimension D_{max} of each molecule is indicated below each molecule and was derived by calculating the pair distance distribution function $P(r)$ from the experimental scattering profiles.

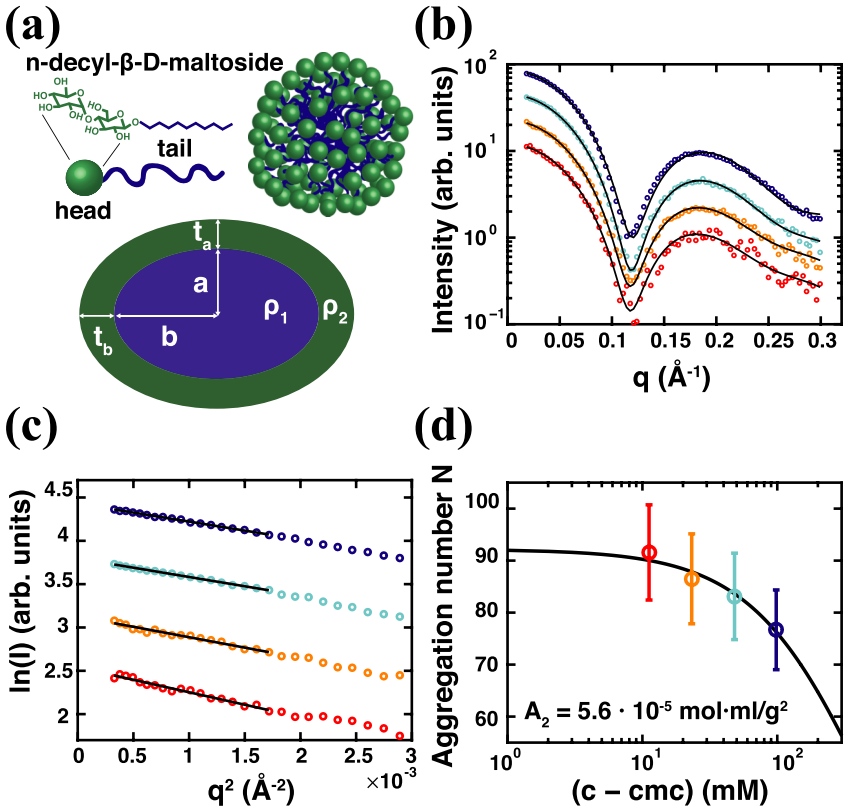

FIG. 6. Characterization of the size, shape, and interactions of DM micelles. (a) Chemical structure of *n*-decyl-β-D-maltoside forming micelles and the schematic of the two-component ellipsoid model. a and b are the dimensions and ρ_1 the electron density of the hydrophobic core. t_a and t_b are the thicknesses and ρ_2 the electron density of the head group region. The figure shows the case of an oblate ellipsoid with a <b. (b) Experimental data for different DM concentrations of 100 mM (blue, top), 50 mM (cyan), 25 mM (orange), and 12.5 mM (red, bottom) and the corresponding fits (black lines). (c) Guinier analysis for DM data shown in (b). (d) Apparent aggregation numbers N obtained from the extrapolated forward scattering intensity and Eq. S2 in the supplementary material[35] (circles, same color code as in (b)). The solid line is a fit to the model of Eq. S6 and A_2 is the fitted second virial coefficient determined from the fit, indicative of weak repulsive interactions between the DM micelles in solution at higher concentrations.

outward and hydrophilic tail groups are segregated in the interior (Fig. 6(a)). Micelle forming detergents are employed in a large range of biochemical and industrial applications. In particular, detergents are commonly used as mimetics of the cell membrane for the solubilization and structural characterization of membrane proteins.[57,58] However, the choice of a suitable detergent for membrane protein solubilization still remains a major hurdle.[59–61] SAXS has been used extensively to characterize the size and shapes of both membrane protein-detergent complexes-formed by a membrane protein surrounded by detergents-and of "empty" micelles.[62–66] To test to what extent our in-house source is capable of revealing the shape and size of detergent micelles, we recorded scattering profiles at different concentrations of *n*-decyl-*β*-D-maltoside (DM), a detergent featuring a maltose head group and a ten carbon single-chain alkyl tail (Fig. 6(a)), which is routinely used for membrane protein solubilization and has been characterized by SAXS in several previous studies.[65,67] We obtain decent signal-to-noise down to a concentration of 12.5 mM DM (Fig. 6(b)). The scattering profiles are well described by a two-component ellipsoid model (Figs. 6(b) and 6(d)), which features a core corresponding to the hydrophobic portion of the micelles formed by the tail groups and of a shell corresponding to the hydrated head groups (Fig. 6(a); see supplementary material for details of the model).[35] The size parameters obtained from the fits of the two-component ellipsoid model reveal oblate micelles with the short axis of the core of ~12.8 Å and the long axes of ~22.2 Å and a thickness of the hydrophilic shell of ~7 Å, in excellent agreement with previous work.[65,67] In addition, we performed a Guinier analysis of the data (Fig. 6(c)) and determined apparent aggregation numbers (i.e., the number of detergent monomers per micelle) from the fitted forward scattering intensities by comparison with a scattering standard as described by Lipfert *et al.* (see supplementary material for details).[35,65] For the measured concentrations, we find radii of gyration in the range of 25.5 Å (±0.4 Å) and aggregation numbers from the forward scattering intensity in the range of ~90 for the lowest concentration (Fig. 6(d)), in excellent agreement with the number calculated from the size of the hydrophic core volume of ~26 nm^3 determined from the two-component ellipsoid fit and with previous measurements, which indicate aggregation numbers in the range of 85–95 monomers per micelle.[65,67] The apparent aggregation numbers show a small, but systematic decrease with increasing detergent concentration (Fig. 6(d)). This decrease in apparent aggregation number could be indicative of DM micelles shrinking with increasing detergent concentrations, which is however unlikely, or due to inter-particle interference effects. The latter results, in particular, from repulsive interactions of the micelles in solution, e.g., due to excluded volume effects, which become more relevant at higher concentrations. Similar decreases in the apparent

aggregation number with increasing detergent concentrations had been seen for a range of uncharged and, in particular, charged detergents previously.[65] Here, we present a new model that describes the apparent aggregation number as a function of detergent concentration in terms of intrinsic, true aggregation number and of the second virial coefficient, a parameter that characterizes the interparticle interactions in solution (see the text and Fig. S5 of the supplementary material).[35] Our DM data are well described by the model (Fig. 6(d), solid line), with a fitted intrinsic aggregation number of $N(c_0) = 92$ and a fitted second virial coefficient of $A_2 = 5.6 \times 10^{-5}$ mol ml/g^2, which indicates weak repulsive interactions. In summary, the DM data suggest that our in-house setup is fully able to reveal the size, shape, and overall interactions of typical detergent micelles.

V. CONCLUSION

We have presented a Mo-anode-based in-house SAXS setup for structural analysis of macromolecules covering a broad range of sizes, shapes, compositions (proteins/DNA/micelles), and scattering properties. Our system contains a Mo-based microfocus X-ray tube with an integrated multilayer mirror delivering a stable monochromatic beam. By using two scatterless slits for collimation, a highly collimated X-ray beam of low beam divergence is generated. The typical flux at the sample stage is around 2.5×10^6 photons/s. Due to the reduced air scattering for Mo-radiation, the sample chambers do not have to be placed in vacuum. Our sample holder contains two sample chambers with observation volumes of 80 μl allowing subsequent automated SAXS measurements of sample and buffer. In addition, the sample chambers can be temperature controlled within a temperature range of 4–70 °C (±0.8 °C). By using the hybrid pixel detector PILATUS 100K, weakly scattering signals can be detected. Our system allows us to perform SAXS measurements on a broad range of weakly scattering biological macromolecules at concentrations comparable to synchrotron based SAXS measurements within 2 h. The achievable scattering vectors for SAXS measurements cover a range of 0.009–0.38 Å^{-1}, such that macromolecules with a size of up to ~30 nm can be structurally characterized. By performing in-house SAXS measurements on a test set of molecules including several proteins and DNA, we demonstrate that the data are of adequate quality to determine *ab initio* low resolution 3D structures of the macromolecules, which were in very good agreement with previously reported structures. Our scattering data were also consistent with theoretical data calculated from the atomic structures of our test molecules. In addition, we demonstrate the instrument's ability to obtain high quality data for detergent micelles commonly used in membrane protein studies and we describe a novel simple model that enables us to determine the micelle aggregation number and second virial coefficient from SAXS data at different detergent concentrations. In general, the significantly lower flux (at least five orders of magnitude) of current Mo-based in-house sources compared to synchrotron sources necessitates much longer integration times (hours compared to seconds, respectively) and limits the practically achievable signal-to-noise ratio, in particular, at larger q values. However, these disadvantages are partially offset by the much greater availability and reduced measurement logistics of an in-house instrument. In summary, our results suggest that Mo-anode-based in-house SAXS experiments are a viable alternative to other anode materials and allow studying many aspects of weakly scattering biological samples.

ACKNOWLEDGMENTS

We thank Dr. Adam Round for support at beamline BM 29 at the ESRF in Grenoble, Dr. Jan Ilavsky (APS) for the calibrated glassy carbon specimen, Dr. Sönke Seifert for support with measurements at beamline 12ID at Argonne National Lab, Dr. Linda Columbus for discussions and for providing detergent samples, and Julian Nguyen for help with the fitting of the micelle data. Use of the Advanced Photon Source was supported by the U.S. Department of Energy, Office of Science, Office of Basic Energy Sciences. The authors acknowledge the Center for Nanoscience (CeNS), DFG-SFB 1032 (Nanoagents) and the Nanosystems Initiative Munich (NIM) for financial support.

[1]J. Lipfert and S. Doniach, Annu. Rev. Biophys. Biomol. Struct. **36**, 307 (2007).
[2]M. H. J. Koch, P. Vachette, and D. I. Svergun, Q. Rev. Biophys. **36**, 147 (2003).
[3]C. D. Putnam, M. Hammel, G. L. Hura, and J. A. Tainer, Q. Rev. Biophys. **40**, 191 (2007).
[4]S. Doniach, Chem. Rev. **101**, 1763 (2001).
[5]A. Guinier, Ann., Phys. (Paris) **12**, 161 (1939).
[6]D. I. Svergun and M. H. J. Koch, Rep. Prog. Phys. **66**, 1735 (2003).
[7]D. I. Svergun, J. Appl. Crystallogr. **25**, 495 (1992).
[8]D. Herschlag, R. Russell, I. S. Millett, and S. Doniach, Nat. Struct. Biol. **7**, 367 (2000).
[9]A. Y. L. Sim, J. Lipfert, D. Herschlag, and S. Doniach, Phys. Rev. E **86**, 021901 (2012).
[10]P. Bernado, E. Mylonas, M. V. Petoukhov, M. Blackledge, and D. I. Svergun, J. Am. Chem. Soc. **129**, 5656 (2007).
[11]D. I. Svergun, Biophys. J. **76**, 2879 (1999).
[12]D. I. Svergun, M. V. Petoukhov, and M. H. J. Koch, Biophys. J. **80**, 2946 (2001).
[13]D. Walther, F. E. Cohen, and S. Doniach, J. Appl. Crystallogr. **33**, 350 (2000).
[14]J. Lipfert, V. B. Chu, Y. Bai, D. Herschlag, and S. Doniach, J. Appl. Crystallogr. **40**, s229 (2007).
[15]J. Lipfert, J. Ouellet, D. G. Norman, S. Doniach, and D. M. J. Lilley, Structure **16**, 1357 (2008).
[16]A. Grishaev, J. Wu, J. Trewhella, and A. Bax, J. Am. Chem. Soc. **127**, 16621 (2005).
[17]J. S. Pedersen, J. Appl. Crystallogr. **37**, 369 (2004).
[18]D. Franke and D. I. Svergun, J. Appl. Crystallogr. **42**, 342 (2009).
[19]G. B. Mortuza, T. Cavazza, M. F. Garcia-Mayoral, D. Hermida, I. Peset, J. G. Pedrero, N. Merino, F. J. Blanco, J. Lyngsø, M. Bruix, J. S. Pedersen, I. Vernos, and G. Montoya, Nat. Commun. **5**, 5072 (2014).
[20]D. M. Dupont, C. K. Thuesen, K. A. Bøtkjær, M. A. Behrens, K. Dam, H. P. Sørensen, J. S. Pedersen, M. Ploug, J. K. Jensen, and P. A. Andreasen, PLoS One **10**, e0119207 (2015).
[21]W. Vogel, Surf. Sci. **156**, 420 (1985).
[22]T. Takamuku, A. Yamaguchi, D. Matsuo, M. Tabata, T. Yamaguchi, T. Otomo, and T. Adachi, J. Phys. Chem. B **105**, 10101 (2001).
[23]M. Matsugami, T. Takamuku, T. Otomo, and T. Yamaguchi, J. Phys. Chem. B **110**, 12372 (2006).
[24]N. Metoki, W. Donner, and H. Zabel, Phys. Rev. B **49**, 17351 (1994).
[25]M. Cianci, J. R. Helliwell, D. Moorcroft, A. Olczak, J. Raftery, and P. J. Rizkallah, J. Appl. Crystallogr. **37**, 555–564 (2004).
[26]T. Mühge, T. Zeidler, Q. Wang, C. Morawe, N. Metoki, and H. Zabel, J. Appl. Phys. **77**, 1055 (1995).

[27]S. Sato, T. Nishi, E. Matsubara, M. Imafuku, N. Nishiyama, Y. Waseda, and A. Inoue, Sci. Technol. Adv. Mater. **3**, 69 (2008).
[28]S. Kuwamoto, S. Akiyama, and T. Fujisawa, J. Synchrotron Radiat. **11**, 462 (2004).
[29]A. Rösler, H.-A. Klok, I. W. Hamley, V. Castelletto, and O. O. Mykhaylyk, Biomacromolecules **4**, 859 (2003).
[30]A. Martel, M. Burghammer, R. J. Davies, E. Di Cola, C. Vendrely, and C. Riekel, J. Am. Chem. Soc. **130**, 17070 (2008).
[31]J. A. Sichert, Y. Tong, N. Mutz, M. Vollmer, S. Fischer, K. Z. Milowska, R. García Cortadella, B. Nickel, C. Cardenas-Daw, J. K. Stolarczyk, A. S. Urban, and J. Feldmann, Nano Lett. **15**, 6521 (2015).
[32]Y. Li, R. Beck, T. Huang, M. C. Choi, and M. Divinagracia, J. Appl. Crystallogr. **41**, 1134 (2008).
[33]A. Bergmann, D. Orthaber, G. Scherf, and O. Glatter, J. Appl. Crystallogr. **33**, 869 (2000).
[34]J. Lipfert, I. S. Millett, S. Seifert, and S. Doniach, Rev. Sci. Instrum. **77**, 046108 (2006).
[35]See supplementary material at http://dx.doi.org/10.1063/1.4940936 for further details on scattering background analysis and detergent micelle characterization.
[36]B. L. Henke, E. M. Gullikson, and J. C. Davis, At. Data Nucl. Data Tables **54**, 181 (1993).
[37]P. Kraft, A. Bergamaschi, C. Broennimann, R. Dinapoli, E. F. Eikenberry, B. Henrich, I. Johnson, A. Mozzanica, C. M. Schlepuetz, P. R. Willmott, and B. Schmitt, J. Synchrotron Radiat. **16**, 368 (2009).
[38]T. N. Blanton, T. C. Huang, H. Toraya, C. R. Hubbard, S. B. Robie, D. Louër, H. E. Göbel, G. Will, R. Gilles, and T. Raftery, Powder Diffr. **10**, 91 (1995).
[39]F. Zhang, J. Ilavsky, G. G. Long, J. P. G. Quintana, A. J. Allen, and P. R. Jemian, Metall. Mater. Trans. A **41**, 1151 (2009).
[40]Y. Bai, R. Das, I. S. Millett, D. Herschlag, and S. Doniach, Proc. Natl. Acad. Sci. U. S. A. **102**, 1035 (2005).
[41]J. Ilavsky, J. Appl. Crystallogr. **45**, 324 (2012).
[42]D. Svergun, C. Barberato, and M. Koch, J. Appl. Crystallogr. **28**, 768 (1995).
[43]H. M. Berman, J. Westbrook, Z. Feng, G. Gilliland, T. N. Bhat, H. Weissig, I. N. Shindyalov, and P. E. Bourne, Nucleic Acids Res. **28**, 235 (2000).
[44]X. J. Lu and W. K. Olson, Nucleic Acids Res. **31**, 5108 (2003).
[45]M. V. Petoukhov, D. Franke, A. V. Shkumatov, G. Tria, A. G. Kikhney, M. Gajda, C. Gorba, H. D. T. Mertens, P. V. Konarev, and D. I. Svergun, J. Appl. Crystallogr. **45**, 342 (2012).
[46]V. V. Volkov and D. I. Svergun, J. Appl. Crystallogr. **36**, 860 (2003).
[47]M. B. Kozin and D. I. Svergun, J. Appl. Crystallogr. **34**, 33 (2001).
[48]W. Wriggers, R. A. Milligan, and J. A. McCammon, J. Struct. Biol. **125**, 185 (1999).
[49]W. Humphrey, A. Dalke, and K. Schulten, J. Mol. Graphics **14**, 33 (1996).
[50]S. Akiyama, S. Takahashi, T. Kimura, K. Ishimori, I. Morishima, Y. Nishikawa, and T. Fujisawa, Proc. Natl. Acad. Sci. U. S. A. **99**, 1329 (2002).
[51]D. J. Segel, A. Bachmann, J. Hofrichter, K. O. Hodgson, S. Doniach, and T. Kiefhaber, J. Mol. Biol. **288**, 489 (1999).
[52]E. Mylonas and D. I. Svergun, J. Appl. Crystallogr. **40**, 245 (2007).
[53]D. J. Segel, A. L. Fink, K. O. Hodgson, and S. Doniach, Biochemistry **37**, 12443 (1998).
[54]P. Chacón, J. F. Díaz, F. Morán, and J. M. Andreu, J. Mol. Biol. **299**, 1289 (2000).
[55]J. J. P. Perry and J. A. Tainer, Methods **59**, 363 (2013).
[56]M. Hammel, Y. Yu, B. L. Mahaney, B. Cai, R. Ye, B. M. Phipps, R. P. Rambo, G. L. Hura, M. Pelikan, S. So, R. M. Abolfath, D. J. Chen, S. P. Lees-Miller, and J. A. Tainer, J. Biol. Chem. **285**, 1414 (2010).
[57]M.le. Maire, P. Champeil, and J. V. Moller, Biochim. Biophys. Acta **1508**, 86 (2000).
[58]S. Hiller, R. G. Garces, T. J. Malia, V. Y. Orekhov, M. Colombini, and G. Wagner, Science **321**, 1206 (2008).
[59]A. M. Seddon, P. Curnow, and P. J. Booth, Biochim. Biophys. Acta **1666**, 105 (2004).
[60]L. Columbus, J. Lipfert, K. Jambunathan, D. A. Fox, A. Y. L. Sim, S. Doniach, and S. A. Lesley, J. Am. Chem. Soc. **131**, 7320 (2009).
[61]J. Bowie, Curr. Opin. Struct. Biol. **11**, 397 (2001).
[62]S. H. Chen, Annu. Rev. Phys. Chem. **37**, 351 (1986).
[63]R. T. Zhang, P. A. Marone, P. Thiyagarajan, and D. M. Tiede, Langmuir **15**, 7510 (1999).
[64]C. Dupuy, X. Auvray, and C. Petipas, Langmuir **13**, 3965 (1997).
[65]J. Lipfert, L. Columbus, V. B. Chu, S. A. Lesley, and S. Doniach, J. Phys. Chem. B **111**, 12427 (2007).
[66]L. Columbus, J. Lipfert, H. Klock, I. Millett, S. Doniach, and S. A. Lesley, Protein Sci. **15**, 961 (2006).
[67]R. C. Oliver, J. Lipfert, D. A. Fox, R. H. Lo, S. Doniach, and L. Columbus, PLoS One **8**, e62488 (2013).